Decision-Directed Slot Synchronization for Pulse-Position-Modulated Optical Signals

M. Srinivasan,[1] V. Vilnrotter,[1] and C. Lee[1]

In this article, we describe a slot-synchronization algorithm for optical signals transmitted using pulse-position modulation (PPM). This algorithm utilizes PPM symbol decisions in order to generate a slot-timing error signal without the use of guard time around the transmitted laser pulse or synchronization symbols. We derive expressions for the open-loop characteristic curve of the error signal and the closed-loop tracking-error variance of this slot synchronizer for an ideal Poisson photon-counting channel. Simulation results for acquisition as well as tracking under a variety of conditions are presented. Finally, the impact on synchronization performance of implementing the transmitted PPM signal through a repetition code is discussed.

I. Introduction

Pulse-position modulation (PPM) has been baselined as the signaling format of choice for deep-space direct-detection optical communications. With this modulation, m bits of information are transmitted via a laser pulse positioned in one of $M = 2^m$ time slots of equal duration, T_s, forming a PPM symbol of duration MT_s. In direct-detection communication systems, the number of photons must be estimated over each slot to form slot observables that are used to make PPM symbol decisions. In order to accurately form the slot observables, however, synchronization between the received PPM slot boundaries and the receiver slot clock must be established and maintained.

In [1], a delay-tracking loop for PPM was analyzed that relied upon a small guard time around the transmitted pulse in order to generate an error signal proportional to the slot-clock delay error. If inclusion of guard time is not an option, some type of decision mechanism must be utilized in order to derive an appropriate error signal. The Mars Laser Communication Demonstration (MLCD) supports slot synchronization through the inclusion of periodic embedded synchronization symbols serving as a pilot signal from which to derive timing information. However, these symbols must be acquired prior to tracking, and their inclusion reduces data throughput. In [2], a synchronizer is described in which slot statistics are tested against a threshold to determine if they should be admitted into the tracking loop. One disadvantage of this approach, however, is that the optimal threshold value depends upon knowledge

[1] Communications Architectures and Research Section.

The research described in this publication was carried out by the Jet Propulsion Laboratory, California Institute of Technology, under a contract with the National Aeronautics and Space Administration.

of the slot statistic parameters. Under changing signal and background conditions, these parameters must be estimated and used to modify the threshold level. Here, we present a slot-synchronizing loop in which the maximum-likelihood PPM symbol decision is used to provide the decision-directed operation allowing an appropriate error signal to be generated. Analysis and simulation results are shown that demonstrate the tracking performance of this algorithm in a photon-counting channel.

II. Decision-Directed Slot Synchronizer

In Fig. 1, we show a transmitted PPM symbol stream with $M = 4$, peak signal intensity λ_s, and background intensity λ_b, with a slot-timing error of Δ. Our objective is to formulate a tracking loop that will detect the presence of the signal pulses and correct the timing error. Figure 2 shows a block diagram of the decision-directed slot synchronizer that we propose. A PPM signal, delayed by the timing error $\Delta > 0$, is passed to the top branch that outputs the integrated slot values and selects the slot corresponding to the maximum value over an arbitrarily defined "pseudo-symbol." In the lower branch, the signal is further delayed by one symbol duration and passed to the error detector, which multiplies it by a "chopping function"—a square wave at the slot frequency—and integrates over time T_s in each slot. The signal is then gated by the slot selector from the upper branch in order to create the timing error signal, which is filtered and then passed to the numerically controlled oscillator (NCO), which outputs the slot clock. Note that symbol synchronization need not be assumed for this algorithm to work. If the initial pseudo-symbol interval contains two signal pulses, there will simply be two main contenders for the maximum slot to be picked by the slot selector, only one of which can be picked to contribute to the error detector. On the other hand, if the pseudo-symbol interval contains no signal pulse, a noise slot will be picked as the maximum, effectively increasing the symbol-error rate (SER) in the PPM decision process. For the discussion in this article, we assume that the pseudo-symbol interval is the same as the true PPM symbol interval, based on the following argument.

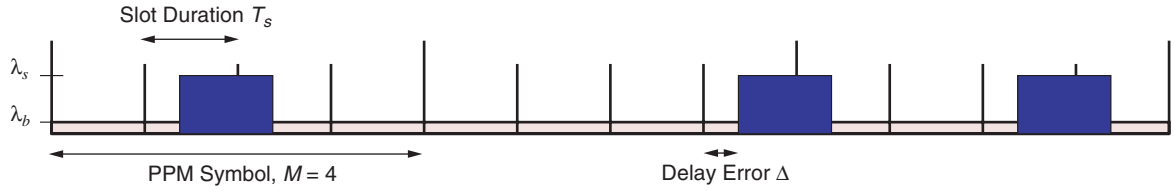

Fig. 1. PPM.

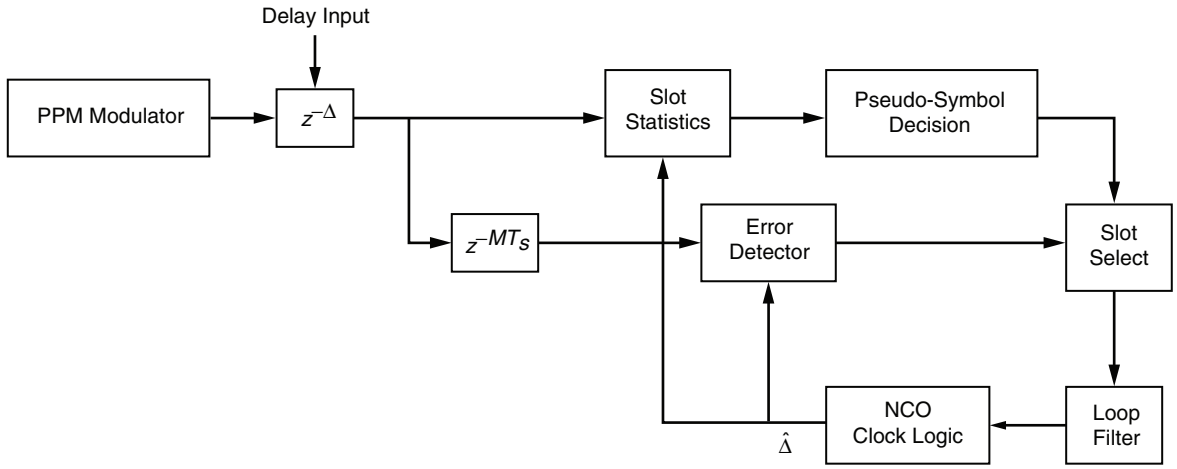

Fig. 2. Block diagram of a slot-synchronization loop for conventional PPM.

If we assume that the beginning boundary of the PPM pseudo-symbol is uniformly distributed within the boundary of a true PPM symbol, then the probability of having a single laser pulse, two laser pulses, or no laser pulse whatsoever within the pseudo-symbol can be computed by first determining the conditional probabilities given each starting offset (measured in slots), and then averaging over the uniform offset distribution. If we denote the symbol offset by Δ_{sym}, then the probability of having a single laser pulse within the pseudo-symbol is given by

$$\begin{aligned} P(1 \text{ pulse}) &= \sum_{i=0}^{M-1} P(\Delta_{sym} = i) P(1 \text{ pulse} | \Delta_{sym} = i) \\ &= \frac{1}{M} \sum_{i=0}^{M-1} \left[\left(1 - \frac{i}{M}\right)^2 + \left(\frac{i}{M}\right)^2 \right] \\ &= \frac{2M^2 + 1}{3M^2} \end{aligned} \tag{1}$$

The probabilities of having either zero or two signal pulses within the pseudo-symbol are equal and given by

$$\begin{aligned} P(0 \text{ pulse}) = P(2 \text{ pulses}) &= \sum_{i=0}^{M-1} P(\Delta_{sym} = i) P(2 \text{ pulses} | \Delta_{sym} = i) \\ &= \frac{1}{M} \sum_{i=0}^{M-1} \left(1 - \frac{i}{M}\right) \frac{i}{M} \\ &= \frac{M^2 - 1}{6M^2} \end{aligned} \tag{2}$$

Equations (1) and (2) show that the probability of having just one pulse is on average roughly four times that of having either zero pulse or two pulses in the absence of symbol synchronization. Therefore, it is reasonable to assume that PPM pseudo-symbols can be approximated by the true PPM symbols for purposes of pulse-detection analysis.

The output of the error detector in the ith slot is the difference between the first and second half of the slot, or

$$e_i(\Delta) = \int_{(i+1/2)T_s}^{(i+1)T_s} y(t)dt - \int_{iT_s}^{(i+1/2)T_s} y(t)dt \tag{3}$$

where $y(t)$ is the delayed received signal (note that for ease of exposition we assume analog signals). If the actual signal pulse is transmitted in the kth slot of a PPM symbol, then the expected value of the error signal is

$$E\big[e_i(\Delta)\big] = \begin{cases} \lambda_s \Delta, & \text{if } i = k \\ -\lambda_s \Delta, & \text{if } i = k+1 \\ 0, & \text{otherwise} \end{cases} = \begin{cases} n_s \delta, & \text{if } i = k \\ -n_s \delta, & \text{if } i = k+1 \\ 0, & \text{otherwise} \end{cases} \tag{4}$$

where $n_s = \lambda_s T_s$ is the mean number of signal photons per signal slot, and $\delta = \Delta/T_s$ is the fractional timing error. The contribution to the error signal from background has been canceled out. For simplicity we have ignored possible signal contributions from the last slot of the previous PPM symbol. Note that in the absence of the slot selector of Fig. 2, Eq. (4) would be averaged over all i slots, resulting in total cancellation of the error signal; slot decisions, therefore, are necessary to generate a useful error signal.

The decision-directed loop allows only the error signal contribution from the maximum value slot in a PPM symbol, or $e_{i^*}(\delta)$, to be fed to the loop filter, where the index i^* corresponding to the maximum-valued slot in a PPM symbol is $i^* = \arg\max_i \int_{iT_s}^{(i+1)T_s} y(t)dt$. Assuming that $\delta > 0$, the unconditional expectation of the error signal over a PPM symbol whose signal occurs in the kth slot is, from Eq. (4),

$$E\big[e(\delta)\big] = E\big[e_k(\delta)\big]P(i^* = k|\delta) + E\big[e_{k+1}(\delta)\big]P(i^* = k+1|\delta) + \sum_{\substack{i=0 \\ i\neq k,k+1}}^{M-1} E\big[e_i(\delta)\big]P(i^* = i|\delta)$$

$$= n_s\delta\big[P(C|\delta) - P(E_1|\delta)\big] \tag{5}$$

where $P(C|\delta) = P(i^* = k|\delta)$ is the probability that the signal slot is maximum, and $P(E_1|\delta) = P(i^* = k+1|\delta)$ is the probability that the slot following the signal slot (also containing some signal energy if $\delta > 0$) is maximum. If $\delta < 0$, $P(E_1|\delta) = P(i^* = k-1|\delta)$. The probabilities in Eq. (5) may be derived from the Poisson PPM symbol-error probability [2] and are given by

$$P(C|\delta) = \frac{e^{-Mn_b - n_s}}{M}$$

$$+ \sum_{n=1}^{\infty} p\big(n; n_b + n_s(1-\delta)\big)p\left(n; n_b + n_s\delta\right) \sum_{l=0}^{M-2} \frac{1}{l+2} \binom{M-2}{l} p\left(n; n_b\right)^l \left(\sum_{j=0}^{n-1} p\left(j; n_b\right)\right)^{M-l-2}$$

$$+ \sum_{n=1}^{\infty} p\big(n; n_b + n_s(1-\delta)\big) \left(\sum_{i=0}^{n-1} p\left(i; n_b + n_s\delta\right)\right) \sum_{l=0}^{M-2} \frac{1}{l+1} \binom{M-2}{l} p\left(n; n_b\right)^l \left(\sum_{j=0}^{n-1} p\left(j; n_b\right)\right)^{M-l-2} \tag{6}$$

and

$$P(E_1|\delta) = P(C|1-\delta) \tag{7}$$

where $p(n;\bar{n}) = \bar{n}^n e^{-\bar{n}}/n!$ (the Poisson probability mass function). The first term in Eq. (6) is the probability of picking the correct signal slot when all slots have zero detected photon counts and a random decision is used to resolve the tie. The second and third terms represent the probabilities that slot k is maximum and the other slots are either lesser in value than slot k or with some subset of l slots tied with slot k, and a random decision is used to resolve the tie. Note that in the second term, slot $k+1$ with mean $n_b + n_s\delta$ is assumed to be tied with slot k, while in the third term, slot $k+1$ is strictly less than slot k. An example of Eq. (5), the error characteristic curve, is shown in Fig. 3, incorporating the probability of correct detection derived in Eq. (6) into the expression.

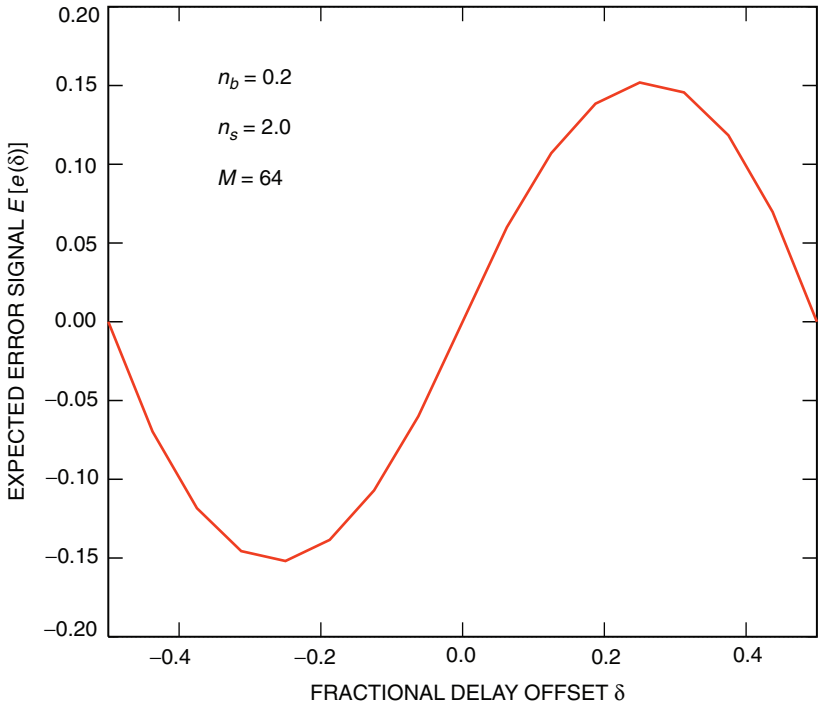

Fig. 3. Theoretical expected value of an open-loop error signal.

A rigorous derivation of the steady-state fractional timing-error variance for this tracking loop would require analysis of the probability density function of the timing-error function, accounting for the effect of the symbol decision process. As an alternative, we obtain an expression heuristically by modifying the following error variance formula [2], which assumes perfect knowledge of the signal slot:

$$\left(\frac{\sigma_\varepsilon}{T_s}\right)^2 = \frac{B_L M}{\lambda_s}\left(1 + \frac{\lambda_b}{\lambda_s}\right) \tag{8}$$

Here $\sigma_\varepsilon^2/T_s^2$ is the fractional variance of the timing error and B_L is the tracking-loop bandwidth. This formula may be modified to account for the effects of signal-slot detection errors by observing that, in the high-data-rate PPM model that we are assuming for this problem, the relatively narrow-band tracking loop does not respond to events occurring on the time scale of PPM symbols, but rather on time scales on the order of the inverse loop bandwidth. For example, a 10-Hz-bandwidth loop implies response times on the order of 100 ms, whereas PPM symbols typically occur on time scales of micro-seconds for data rates on the order of megabits per second. Therefore, we may analyze the loop response by considering a long string of PPM symbols satisfying the above constraints. If we define the estimated order of a string of N consecutive PPM symbols as the number of "true" signal pulses observed over the NM slots contained therein, then if no symbol detection errors occur, the estimated order is $NM/N = M$. On the other hand, if symbol detection errors are made and $K < N$ true signal pulses are detected, the estimate of the PPM order is $NM/K > M$. In cases where N is sufficiently large (as in our case), K/N is equal to the probability of correct detection, $P_c = P(C|\delta \approx 0)$. Using this argument, we replace M in Eq. (8) with $NM/K = M/P_c$, leading to the following expression:

$$\left(\frac{\sigma_\varepsilon}{T_s}\right)^2 = \frac{B_L M}{\lambda_s P_c}\left(1 + \frac{\lambda_b}{\lambda_s}\right) \tag{9}$$

Rewriting this in terms of the average signal intensity $\bar{\lambda}_s = \lambda_s/M$, we obtain

$$\left(\frac{\sigma_\varepsilon}{T_s}\right)^2 = \frac{B_L}{\bar{\lambda}_s P_c}\left(1 + \frac{\lambda_b}{M\bar{\lambda}_s}\right) \tag{10}$$

Note that we also can derive the tracking variance when embedded tracking symbols inserted every L PPM symbols are used in the synchronizer of Fig. 2 in place of decision-derived symbols. We simply use Eq. (8), replacing M with LM, giving us

$$\left(\frac{\sigma_\varepsilon}{T_s}\right)^2 = \frac{B_L ML}{\lambda_s}\left(1 + \frac{\lambda_b}{\lambda_s}\right) = \frac{B_L L}{\bar{\lambda}_s}\left(1 + \frac{\lambda_b}{M\bar{\lambda}_s}\right) \tag{11}$$

From Eqs. (10) and (11), one can conclude that the use of embedded synchronization symbols outperforms the decision-directed algorithm in terms of tracking performance only if the frequency of embedded symbols $1/L$ is greater than P_c. On the other hand, insertion of embedded symbols always results in a degradation of information throughput.

III. Performance Results

A discrete-time Matlab simulink simulation of the algorithm was performed in order to test acquisition and tracking performance of the decision-directed slot synchronizer. An idealized Poisson model of the photodetector was assumed, with fixed signal and background photon arrival rates and static phase offsets. Initially, a first-order loop (loop filter $F(z) = 1$) was used, along with 64 samples per PPM slot. In practice, fewer samples per slot typically may be used, along with an interpolation filter to provide greater resolution timing correction [3]. Finally, for the purposes of these simulations, symbol boundaries were known, although in fact symbol timing usually is obtained only subsequently to slot synchronization. As mentioned earlier, this knowledge is not necessary to the algorithm; however, lack of symbol synchronization generally will degrade the steady-state tracking error as well as increase the acquisition time. In principle, one could analytically determine the extent of degradation by calculating the symbol-error probability conditioned on each possible symbol misalignment value (in slots), and then average as in Eq. (5) to arrive at the mean error signal independent of symbol timing. Our analysis from Section II did show, however, that it is justifiable to analyze performance by assuming symbol synchronization.

In our first set of simulations, we assume 64-PPM, $T_s = 40$ ns, mean number of background photons per slot $n_b = \lambda_b T_s = 9$, and first-order loop bandwidth $B_L = 10$ Hz. The mean number of signal photons per pulse, $n_s = \lambda_s T_s$, ranges from 2 to 10, and static initial timing delays of $T_s/4$ and $T_s/2$ are used. Phase output plots for these two initial delay values are shown in Fig. 4, demonstrating convergence to the desired timing offsets. In Fig. 5, we plot the fractional error variance from Eq. (9) along with measured variances from the simulation results obtained once the loop has acquired for the two initial delay values, showing reasonable agreement between analysis and simulation. The error variance results are also tabulated in Table 1, along with acquisition times and uncoded symbol-error rates.

The acquisition time for a first-order error-tracking loop is proportional to the inverse loop bandwidth, i.e., $T_{\text{acq}} \propto 1/B_L$, if a uniform distribution on the initial phase error is assumed [4]. In the decision-directed loop, the acquisition time is expected to be somewhat longer due to the erroneous symbol decisions that do not contribute to the derivation of a useful error signal. Accounting for this by reducing the loop bandwidth by the percentage of correct symbol decisions, or P_c, we can argue that

$$T_{\text{acq}} \propto \frac{1}{B_L P_c} \tag{12}$$

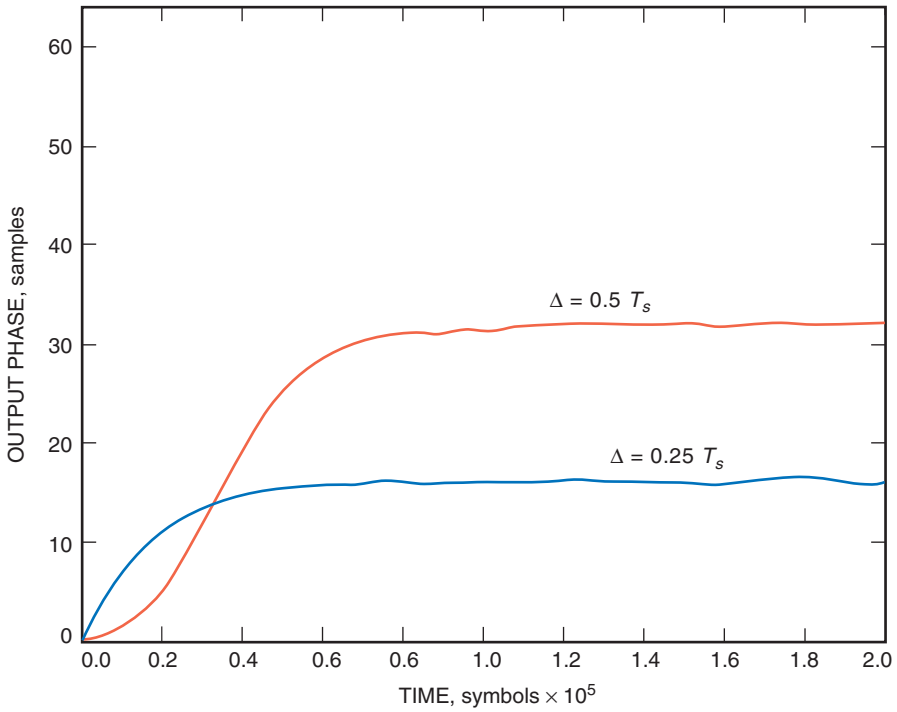

Fig. 4. Phase output from the simulated slot synchronizer (first-order loop): 64-PPM, T_S = 40 ns, n_b = 9, B_L = 10 Hz, 64 samples per slot.

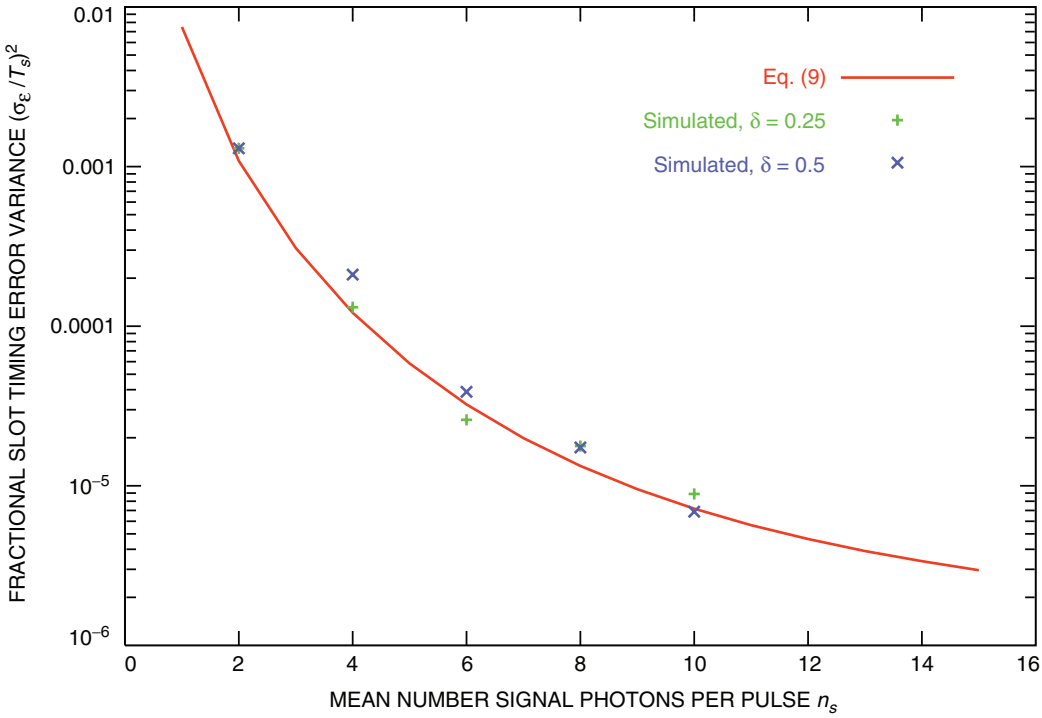

Fig. 5. Fractional timing-error variance (first-order loop): 64-PPM, T_s = 40 ns, n_b = 9, B_L = 10 Hz, 64 samples per slot.

Table 1. Simulation data: 64-PPM, $T_s = 40$ ns, $n_b = 9$, $B_L = 10$ Hz, 64 samples per slot.

n_b	n_s	Δ/T_s	T_{acq}, s		$(\sigma_\varepsilon/T_s)^2$		SER
			Simulation	Eq. (12)	Simulation	Eq. (9)	
9	10	0.25	0.1413	0.1479	8.9×10^{-6}	7.19×10^{-6}	0.324
		0.5	0.2782		6.88×10^{-6}		
9	8	0.25	0.22	0.196	1.77×10^{-5}	1.33×10^{-5}	0.49
		0.5	0.619		1.74×10^{-5}		
9	6	0.25	0.2432	0.3033	2.59×10^{-5}	3.23×10^{-5}	0.67
		0.5	0.3122		3.88×10^{-5}		
9	4	0.25	0.7378	0.584	1.31×10^{-4}	1.22×10^{-4}	0.829
		0.5	1.498		2.10×10^{-4}		
9	2	0.25	2.048	1.54	0.0013	1.08×10^{-3}	0.935
		0.5	2.432		0.0013		

As we see in Fig. 3, however, an unstable equilibrium point exists at a delay offset of half a slot. The small restoring force at this initial offset can result in acquisition times that are two to three times larger than the average acquisition time, as can be seen in Table 1, which tabulates the simulation acquisition time results. Note that at even the highest SER the decision-directed algorithm is able to lock in and track the slot clock.

A second set of simulations was performed for conditions more similar to an MLCD mission operating point. In order to track a frequency offset, a second-order loop was used, with a digital loop filter having frequency response $F(z) = G_1 + G_2/(1 - z^{-1})$, where G_1 and G_2 are functions of the loop gain, bandwidth, and update time [5]. These simulations also used 64-PPM but have $n_b = 0.0025$, n_s ranging from one to four, and 1.6-ns slots, corresponding to the narrow slot widths used in the MLCD mission. Per typical hardware specifications [3], only four samples per slot were used here, along with an interpolation filter to adjust the fine-timing resolution. Figure 6 shows the resulting data for the two initial fractional timing offsets of 0.25 and 0.5, as well as a case with a frequency offset of 100 Hz, demonstrating the ability of the second-order loop to track the frequency offset, as shown from the phase-error plot of Fig. 7. We note here that the simulated tracking-error variances do not match the analytical expression as well as in the first-order case. There may be a number of reasons for this. The operating point is different, so that some of the assumptions used to derive Eq. (9) may not hold. The fact that this is a second-order loop and the inclusion of an interpolation filter also may affect the digital loop transfer function and loop gain in such a way that the actual loop bandwidth does not match the design loop bandwidth used to set the loop filter coefficients. In any case, further analysis is merited to resolve this discrepancy.

IV. Synchronization of Repeat-Coded PPM

The results presented in the previous sections assume use of conventional contiguous PPM symbols, as in Fig. 1. The signaling structure for MLCD, however, calls for use of repeat-coded PPM symbols to implement longer slot durations in order to overcome limitations of the transmitting laser.[2] Figure 8 shows an example of repeat-coded PPM. Here we discuss the impact of the repeat-coded symbols upon performance of the decision-directed synchronizer. We refer to the underlying transmitted slot of duration $\tilde{T}_s$ as the "primitive" slot, and the corresponding M-ary PPM symbol with slot duration $\tilde{T}_s$ as the primitive PPM symbol. The original PPM symbol is transmitted by repeating R of the primitive PPM symbols, all having the same pulse location. Each primitive symbol has the same average signal intensity

[2] *Mars Laser Communications Demonstration ICD*, draft (internal document), Jet Propulsion Laboratory, Pasadena, California, 2005.

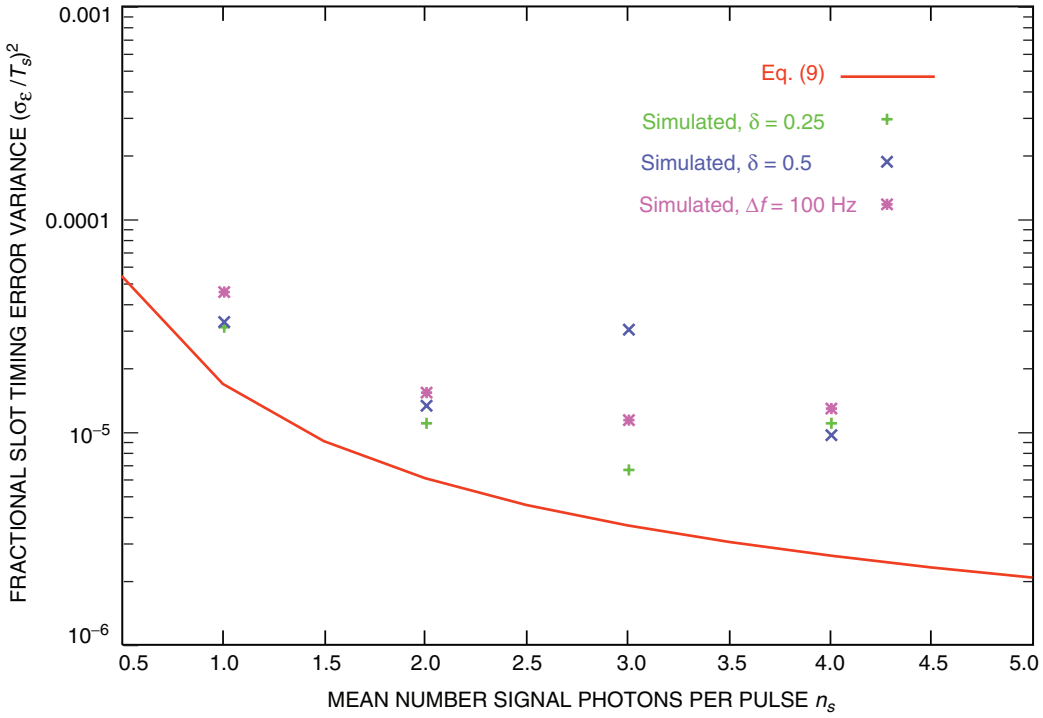

Fig. 6. Fractional timing-error variance (second-order loop):
64-PPM, T_s = 1.6 ns, n_b = 0.0025, B_L = 100 Hz, 4 samples per slot.

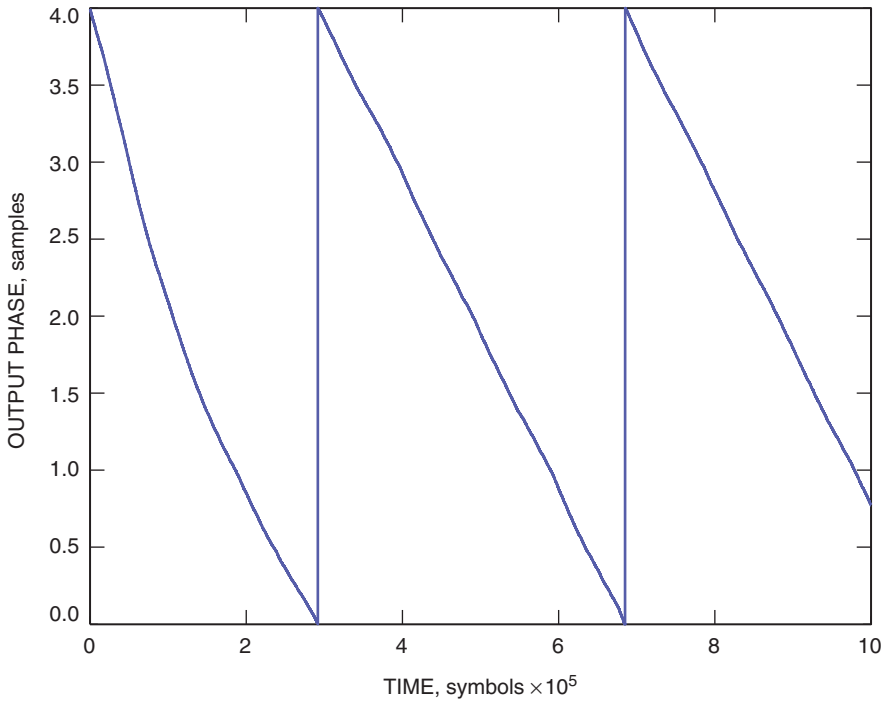

Fig. 7. Phase output from simulated slot synchronizer (second-order loop):
64-PPM, T_s = 1.6 ns, n_b = 0.0025, B_L = 100 Hz, Δf = 100 Hz, 4 samples per slot.

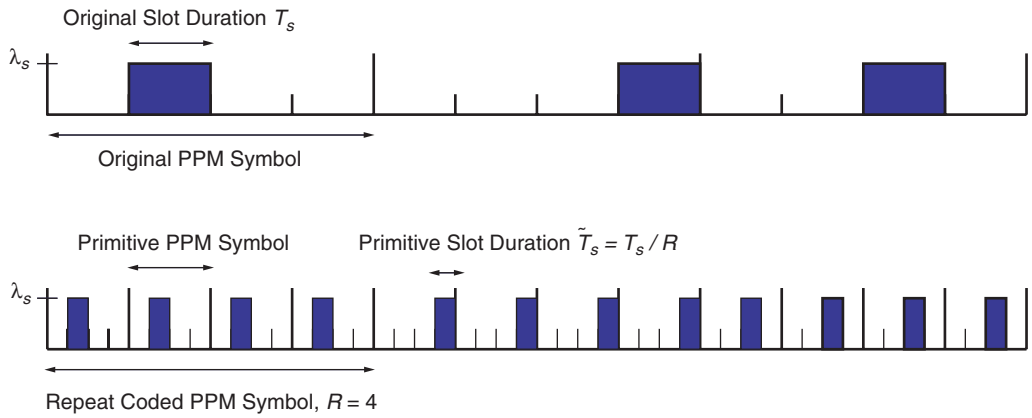

Fig. 8. Repeat-coded PPM symbols.

as the original, λ_s, but shorter pulse duration, so that the mean number of signal photons per original PPM symbol pulse, n_s, is divided equally into the R primitive symbol pulses. The order R repeat-coded PPM symbol has "effective" slot duration $T_s = R\tilde{T}_s$.

Upon acquisition of the repeat code, the receiver forms the sum of the slot statistics from the ith primitive slots of the R primitive PPM symbols over a repeat-code block, and then forms the likelihood ratio for the ith slot of the repeat-coded PPM symbol from this sum to pass on to the decoder, for $0 \leq i \leq M-1$. Likewise, once slot acquisition has been performed, the decision-directed slot-synchronization loop makes a decision based on the repeat-coded PPM symbol (as opposed to the primitive symbol), as shown in Fig. 9. The primitive PPM symbols, delayed by some timing error Δ, are passed to the top branch that forms the integrated primitive slot values, combines them over the repeat-code block, and selects the slot corresponding to the maximum value. In the lower branch, the signal is further delayed by a repeat-coded symbol duration and is passed to the error detector, which multiplies it by a square wave at the primitive slot frequency—and integrates over the primitive slot. This signal then is gated by the slot selector from the upper branch in order to create the timing-error signal, which is filtered and then passed to the NCO that outputs the primitive slot clock.

We see from Eq. (9) that the timing error as a fraction of the slot duration is a function of the signal and background arrival rates, the loop bandwidth, the PPM order, and the probability of making a correct symbol decision, which is itself a function of the signal and background photon arrival rates, the PPM order, and the slot duration. Therefore, all other parameters being fixed, a reduction in the slot duration ordinarily would decrease P_c, thereby increasing the error variance. However, as our PPM symbol decision for the slot-synchronization loop is made over the repeat-coded symbol, whose duration $MT_s = MR\tilde{T}_s$ remains constant (the repeat-code order R increasing with decreased primitive slot duration), P_c should remain fixed as well, assuming negligible loss in combining the primitive PPM symbols to make the decision. So theoretically, the implementation of the repeat code should not impact the slot statistics delivered to the decoder.

We now want to examine the impact of slot synchronization of repeat-coded PPM symbols on the detection statistics used in forming likelihood ratios for the decoding process. Let σ_{big} and $T_{\text{big}} = T_s$ refer to the rms tracking error and slot duration of a non-repeat-coded symbol, and σ_{small} and $T_{\text{small}} = \tilde{T}_s$ refer to the same parameters for a primitive symbol. Let σ_{rep} be the rms timing error on the detection statistic formed from the combined repeat-coded symbol. Denote the zero mean timing delay on a primitive slot by the random variable Δ. We know from Eq. (9) that if the PPM symbol decisions are made over the entire repeat-code block, then

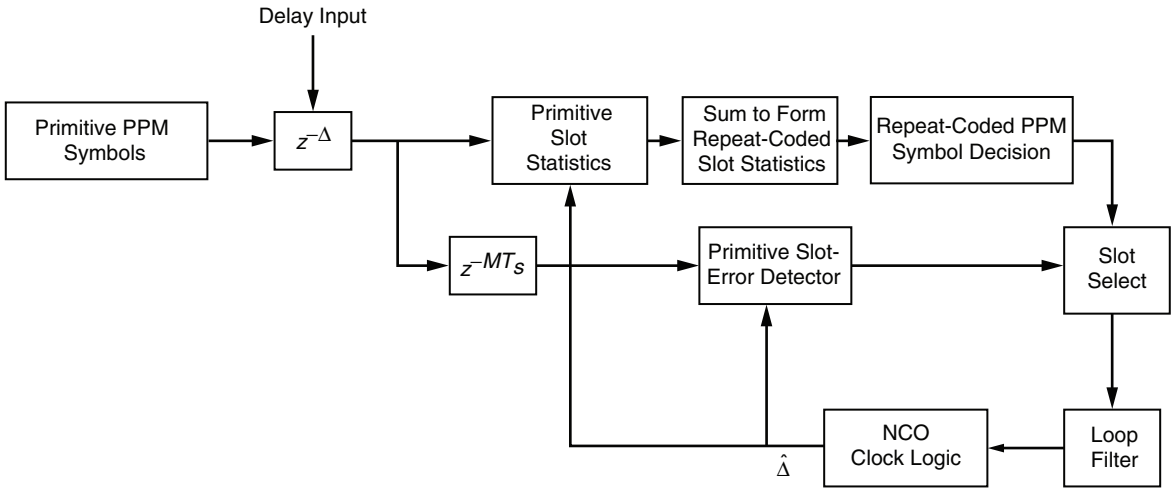

Fig. 9. Block diagram of a slot-synchronization loop for repeat-coded PPM.

$$\left(\frac{\sigma_{\text{big}}}{T_{\text{big}}}\right)^2 = \left(\frac{\sigma_{\text{small}}}{T_{\text{small}}}\right)^2 \tag{13}$$

where $T_{\text{small}} = T_{\text{big}}/R$. The decoder likelihood ratio for the ith PPM slot is given by

$$LR(i) = e^{-n_s}\left(1 + \frac{n_s}{n_b}\right)^{Y(i)} \tag{14}$$

where $Y(i)$ is the detected observable in the ith slot. In the case of repeat-coded PPM, $Y(i) = \sum_{j=1}^{R} X_j(i)$, where $X_j(i)$ is the detected observable in the ith slot of the jth primitive PPM symbol. Now $X_j(i)$ is Poisson with parameter $\lambda_b T_{\text{small}} + \lambda_s(T_{\text{small}} - \Delta)$ for a given timing error Δ. Therefore, $Y(i)$ is also Poisson with parameter $R\lambda_b T_{\text{small}} + R\lambda_s(T_{\text{small}} - \Delta) = \lambda_b T_{\text{big}} + \lambda_s(T_{\text{big}} - R\Delta)$, since for tracking we assume that the loop bandwidth is narrow enough that all of the primitive slots see the same value of Δ. We interpret this to mean that the timing error on the combined statistic $Y(i)$ is R times as large as on the primitive slot statistic $X_j(i)$, and the variance on that timing error, σ^2_{rep}, is given by the variance of $R\Delta$. We then have

$$\sigma^2_{rep} = \text{Var}\left[(R\Delta)^2\right] = R^2\sigma^2_{\text{small}}$$

$$= R^2\left(\frac{T_{\text{small}}}{T_{\text{big}}}\right)^2\sigma^2_{\text{big}}$$

$$= \sigma^2_{\text{big}}$$

So theoretically, the implementation of the repeat code should not change the loss on the detection statistic due to slot-synchronization tracking errors. On the other hand, acquisition likely will be affected by a short primitive slot duration.

V. Conclusions

A decision-directed algorithm was presented for slot synchronization in PPM signals. Expressions for the error characteristic curve and tracking error variance were derived, and simulations were performed, showing good agreement for the first-order loop. The loop was shown to track under conditions similar to those present in the Mars Laser Communication Demonstration, including a frequency offset. Finally, it was argued that the implementation of repeat-coded PPM does not affect the tracking performance of this algorithm.

References

[1] V. A. Vilnrotter, E. R. Rodemich, and H. H. Tan, "A Synchronization Technique for Optical PPM Signals," *The Telecommunications and Data Acquisition Progress Report 42-87, July–September 1986*, Jet Propulsion Laboratory, Pasadena, California, pp. 24–31, November 15, 1986.
http://tmo.jpl.nasa.gov/tmo/progress_report/42-87/87C.PDF

[2] R. M. Gagliardi and S. Karp, *Optical Communications*, New York: John Wiley and Sons, Inc., 1995.

[3] A. A. Gray and C. Lee, "Discrete-Time Demodulator Architectures for Free-Space Broadband Optical Pulse-Position Modulation," *The Interplanetary Network Progress Report*, vol. 42-158, Jet Propulsion Laboratory, Pasadena, California, pp. 1–45, August 15, 2004.
http://ipnpr.jpl.nasa.gov/tmo/progress_report/42-158/158I.pdf

[4] H. Meyr, M. Moeneclaey, and S. A. Fechtel, *Digital Communication Receivers, Vol. 2: Synchronization, Channel Estimation, and Signal Processing*, New York: Wiley-Interscience, October 1987.

[5] S. Aguirre, W. J. Hurd, R. Kumar, and J. Statman, "A Comparison of Methods for DPLL Loop Filter Design," *The Telecommunications and Data Acquisition Progress Report 42-87, July–September 1986*, Jet Propulsion Laboratory, Pasadena, California, pp. 114-124, November 15, 1986.
http://tmo.jpl.nasa.gov/tmo/progress_report/42-87/87M.PDF